ITB Graduate School Conference (IGSC) ISSN: 2963-718X
December 21, 2021

Spatial Distribution of Radon Gas Concentration by Considering the Lineament Densities Extracted from Digital Elevation Model (DEM) at Patuha Geothermal Field, West Java, Indonesia

Fikriansyah Ersyad[1], Mohamad Nur Heriawan[2*] & Irwan Iskandar[2]

[1]Master Program of Mining Engineering, Faculty of Mining and Petroleum Engineering, Bandung Institute of Technology, Bandung, Indonesia
[2]Research Group of Earth Resources Exploration, Faculty of Mining and Petroleum Engineering, Bandung Institute of Technology, Bandung, Indonesia
Email: fikrians.ersyad@outlook.com
*Corresponding author e-mail: heriawan@mining.itb.ac.id

Abstract. Soil radon measurements is a technique that can be used for geothermal prospecting. In general, the concentration of Radon-222 (Rn) gas is associated with the fractures and faults traces. This study aims to modeling the near-surface permeability zone based on the spatial correlation between Rn gas concentrations as the primary variable and lineament structural density as the secondary variable by using multivariate geostatistical method named Ordinary Cokriging (COK) and Ordinary Kriging (OK). Radon gas concentrations were measured from 17 shallow drill holes and were collected over nine periods during 2020. In this study, the Digital Elevation Model (DEM) with 8.3-m resolution were extracted to produce three lineaments structural densities i.e., frequency, length, and intersection by using modified Segment Tracing Algorithm (m-STA) method which coverage area of 3.16 × 4.78 km. The three lineament density maps with grid dimension were generated. The major direction of lineament structural was in N85°E and N315°E which is like the major direction of regional and local faults in the study site. Three radon measurement sites i.e., TTN01, TTN02, and PA04 which is in the northern site showed higher concentration, while other sites mainly in northeastern and southern sites showed lower concentration. This methodology was applied in Patuha Geothermal Field (PGF), West Java, Indonesia.

Keywords: *COK; lineament density; m-STA; radon concentration; permeability zone; OK.*

1 Introduction

Indonesia has an enormous of geothermal potential in the world since the location of the country is in the ring of fire in volcano line and makes Indonesia was considered the world's richest geothermal with approximately 28.91 GW of geothermal energy potential is spread across in 312 locations on several islands such as Java, Sumatra, Bali, Nusa Tenggara and Sulawesi (Nugroho, 2018). However, the utilization ratio of this potential is immensely small, less than 5%.

Geothermal fluids are the prime geothermal resource for power generation. The fluids are mostly contained in highly permeable fractures that control their flow (Nielson, 1997; Tamanyu et al., 1998). Permeable fractures form fluid paths and induce fluid circulation (Morris et al., 1996; Diaz and Arias, 2020), which leads to the evolution of the geothermal system and fluid water chemistry (Rowland and Sibson, 2004; Brogi and Novellino, 2015). Highly permeable zones are therefore chosen as the main target for geothermal exploration.

Extracted lineament by Modified Segment Tracing Analysis (m-STA) using data Digital Elevation Model (DEM) simplify helps in preliminary exploration to detect permeable zones and correlate with regional or local fault patterns which is contribute important information for prospect areas and characterization of geologic structure in geothermal field. Fractures and faults may partially appear on aerial photographs, satellite images and/or digital terrain model (DTM) as lineaments. Satellite images data which had been mentioned ages in in the field of geology can be divided broadly into three categories like lineament enhancement and lineament extraction for characterization of geologic structure (O'Leary and Simpson, 1977); image classification to perform geologic mapping or to locate spectrally anomalous zones attributable to mineralization (Hook et al., 1991); and superposition of satellite images and multiple data such as geological information system (Moon et al.,1991). Lineament detection is automatically referred to extraction which is carried out based on the examination of digital numbers from satellite images with certain criteria, for example by using the m-STA (modified Segment Tracing Algorithm) method. The m-STA works based on the STA principle (Koike et al., 1995). The STA principle detects lines from pixels that are read as vector elements by examining local variations in the gray level of digital numbers (Saepuloh, 2020). Segment Tracing Analysis (STA) was used to identify lineaments that showed an ascending path function of hydrothermal fluids in active volcanic area (Koike et al., 1998). Lineament using data m-STA and density distribution particularly can be used to cover by lacking Radon (Rn) data for mapping of permeable zones.

Geothermal prospecting by ground Radon (Rn) measurements showed that radon was associated with fault traces and indicated general regions of higher radon concentrations which probably indicated favorable areas for drilling for geothermal steam (Whitehead, 1984). Studied by Whitehead (1981) showed that there was an apparently higher level of Rn in the ground near existing geothermal bores in a producing field probably due to the heat in the ground from the bore since radon diffuses faster when thermal gradient exists. Geochemical measurement of dissolved radionuclide concentrations in air, soil and gases is the most desirable method for geothermal evaluation and exploration. The usefulness of such geochemical methods has been shown to assess geothermal potential, the origin of the fluids, and the structure of the aquifer into which the fluid rises.

Applications of Rn measurements include spatial and temporal changes in Rn concentration in response to reservoir thermodynamic conditions and estimation of fluid flow and circulation in hydrothermal systems.

Based on that background, this study aims to clarify and can optimize the presence of high permeability zones near the surface which is a key point for the existence of steam spots while reducing geological risks in development exploration by considering spatial distribution of Radon gas concentrations with lineaments data by m-STA and for modeling of permeability zones by Rn concentrations and lineaments structural densities i.e., frequency, length, and intersection. The above methods were applied to the Patuha Geothermal Field (PGF), West Java, Indonesia.

2 Study Site

The PGF are administratively located in the Bandung regency, West Java at coordinates 7°10'36,7″ Latitude and 107°24'30,7″ BT. The PGF system has a vapor-dominated reservoir. There are many geothermal manifestations near Patuha such as fumaroles, with a temperature of 93°C, acidic hot springs and hydrothermal alteration. The hot springs are located around northern Patuha and have temperatures ranging from 35 to 83°C and the water flow between 2-15 l/s (Nugroho, 2018).

2.1 Accessibility

The accessibility to the PGF is about 2.5 hours and it is about 50 km southwest of the Bandung city by using a car via a graded dirt road from the town of Ciwidey. The elevation in Patuha geothermal field is about 1800 to 2000 meters a.s.l. The cool, rainy climate in the mountains supports a mix of tropical rain forest and government-run tea plantations.

2.2 Regional Geology

The geothermal resource at PGF is associated with arc volcanism resulting from subduction of the Indo - Australian plate beneath the Eurasian plate at the Java Trench. The PGF is located within a volcanic highland composed of andesitic lavas and pyroclastic of late-Tertiary to Quaternary volcanic belt along the island of Java with many active volcanoes (Sriwana et al., 2001). The PGF system hosts a vapor-dominated or two-phase reservoir that is penetrated by two volcanic chimneys containing magmatic waters (Raharjo et al., 2016). The basement is composed of Tertiary volcanic rocks with micro-diorite an epidote-rich zone formed under the silicification and propylitization zones suggests advanced hydrothermal alteration at 200 °C or higher at around 1,200 m above the sea level (a.s.l.), and an argillic zone is

developed under the near-surface weathered zone (WestJEC, 2007). Regional geology of study area can be shown at Figure 1.

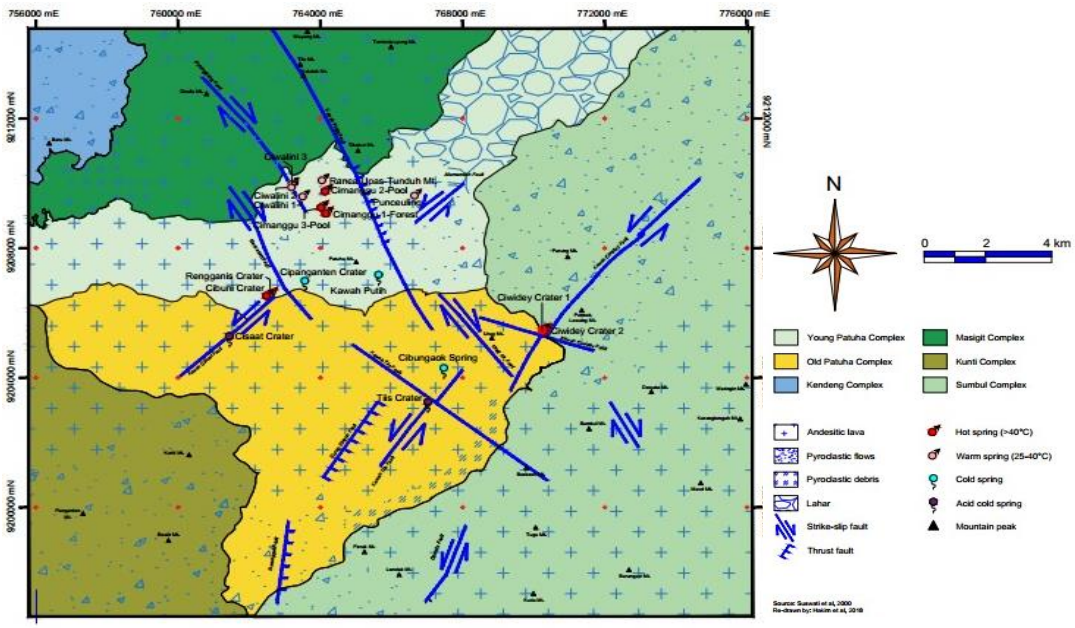

Figure 1 Geology and sampling site maps of the Patuha Geothermal Field (PGF, showing that the PGF is mainly covered by andesitic and volcanic products. Mapped by (Suswati et al., 2000). The coordinate system used is UTM zone 48s.

3 Material and Methods

3.1 Radon Gas Concentration Monitoring Data

Radon gas concentrations were measured from 17 shallow drill holes using radon detector RAD 7 and were collected over nine periods during 2020 in the PGF and were divide in cycle: (1) 14 – 27 July 2020; (2) 6 – 8 August 2020; (3) 14 – 16 August 2020; (4) 28 – 30 August 2020; (5) 24 – 28 August 2020; (6) 3 – 4 October 2020; (7) 28 – 29 October 2020; (8) 12 – 16 November 2020; (9) 17 – 19 December 2020. Radon gases were measured in the locations which is shown in Figure 2.

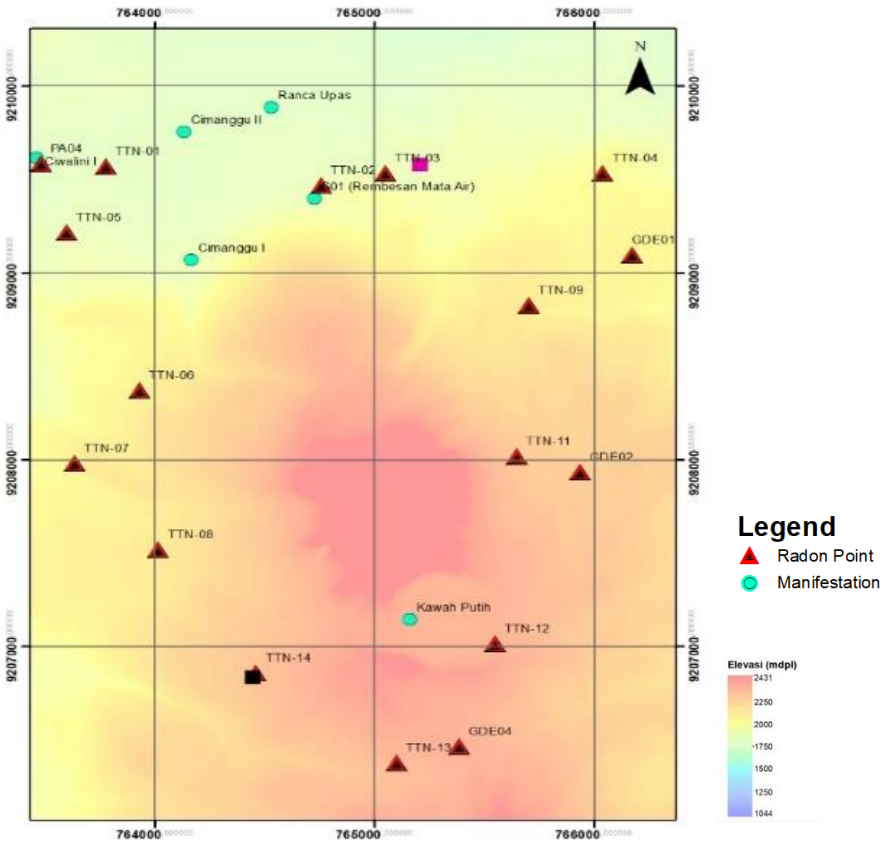

Figure 2 Location measurement and monitoring data radon gas concentrations.

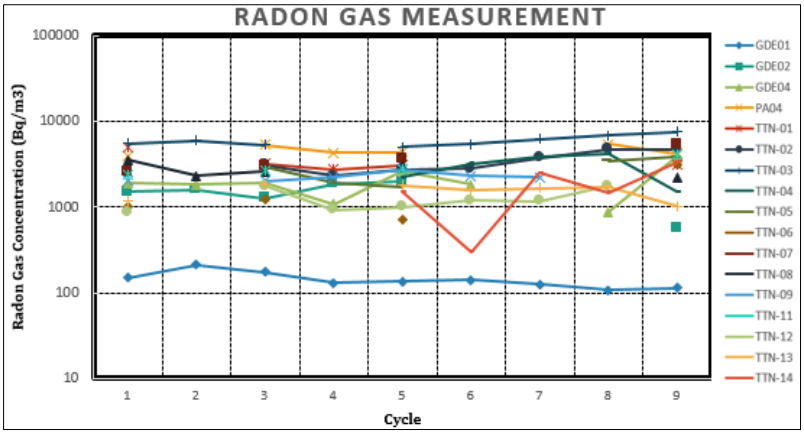

Figure 3 Radon gas concentrations data at each shallow drill hole over nine periods in the PGF.

3.2 Modified Segment Tracing Algorithm for Extracting the Lineament

Lineament analysis using satellite imagery and DEM have been widely applied to the exploration of fracture-related resources and characterization of crust fracture systems (Saepuloh et al., 2018) because regional lineaments are commonly interpreted as surface expressions of geologically weak zones, such as faults and fractures (Masoud and Koike, 2011). Lineament extraction process from the DEM data and m-STA is based on providing with a specific illumination interval. The difference in lighting direction results in two multi-shaded reflection DEM images. Extracting lineaments by m-STA can be applied from low-contrast zones in shadows (i.e., small relief) and lineaments parallel to the illumination direction. After extracting the lineaments from each image, the overlapped lineaments were merged into one lineament. Short lineaments with a starting point closely located to the endpoint of another lineament with similar directions were grouped and connected (Heriawan et al., 2021).

The lineament distribution is characterized using a rose diagram, which shows the directional frequency of the extracted lineaments by the lineament frequency (i.e., number of the lineaments per total number) in each 10° sector, and a lineament density map. After griding the entire study by cells, the lineament density, LD, is defined as the total number of lineaments in a unit cell (lines/km^2).

3.3 Geostatistical Methods

Geostatistics is a statistical science that integrates spatial continuity to model a regional variable. This spatial estimation technique is widely used in the mining industry such as mineral resource estimation, model uncertainty estimation, risk quantification, sampling distance estimation or optimal drilling. The concept of geostatistics is based on a regional variable which is a function of z(x). This function represents the value at a point (x) in space. Variogram or semivariogram is an analytical tool in geostatistics to measure spatial continuity or pattern of similarity of regional variables. To improve the Rn concentration distribution estimation by considering the correlation between Rn concentration and lineament density at location x, in this study Ordinary Kriging (OK) and Ordinary Cokriging (COK) methods were applied.

3.3.1 Ordinary Kriging Method

Kriging in essence a generalized linear regression algorithm extending the data-to-unknown correlation to data-to-data correlation through a non-diagonal kriging matrix. It is a regression with non-independent data: actually, it can be shown that kriging consist, first of decorrelating the data by defining linear combinations of the original data that are orthogonal for a given covariance or

variogram model, then of a traditional linear regression from these "independent" data transform (Journel, 1989). In OK the expected value of the random function is locally re-estimated from local data, while the covariance model is kept stationary. The OK concept has been extended to local estimation of the parameters of a functional trend. The corresponding estimate in OK expression (Journel and Huijbregts, 1978):

$$z_{OK}^{*}(u) = \sum_{\alpha=1}^{n(u)} \lambda_{\alpha}^{OK}\ (u) z(u_{\alpha}) \quad (1)$$

where the kriging weights sum to 1: $\sum_{\alpha=1}^{n(u)} \lambda_{\alpha}^{OK}\ (u) = 1$

The OK method is the most widely used kriging method. It serves to estimates the value at an arbitrary point within a region using a known semivariogram and data from the area surrounding the point (Wackernagel, 2003). OK is adopted by assuming the stationarity of the displacement data field, i.e., constant mean of the displacement data and dependance of the data covariance only on the separation distance (e.g., Wackernagel, 2003). Variogram or semivariogram is an analytical tool in geostatistics to measure the spatial continuity or polarity of regional variables. The variogram equation (Rossi and Deustch, 2014) is described as:

$$\gamma(\mathrm{h}) = \frac{1}{2N\ (h)} \sum_{i=1}^{N} [(z(x_i) - \ (z(x_{i+h})]^2 \quad (2)$$

As the experimental semivariograms of the three index data exhibited local stationarity, OK was confirmed as an appropriate spatial estimator in this study.

3.3.2 Ordinary Cokriging Method

Ordinary Cokriging (COK) method is the extension of the kriging paradigm to estimation of one attribute using data related to other attributes. This COK is type of geostatistical multivariate incorporates other variables in the estimation process (primary variable – secondary variable) which is named covariable. Primary variable data usually has less data than secondary variables. The COK method which is commonly used to incorporate co-variable spatial correlations into estimates. There are two types of cokriging was usually used to alleviate the burden of modeling all the variograms with linear model of coregionalization, both are Markov Model 1 (MM1) and Markov Model 2 (MM2) (Journel, 1999). MM1 takes Markov-type screening hypothesis:

$$\mathrm{E}\{Z_2(u) \mid Z_1(u);\ Z_1(u+h) = \mathrm{E}\{Z_2(u) \mid Z_1(u)\} \quad (3)$$

i.e. the dependence of the secondary variable on the primary is limited to the co-located primary variable. The cross-covariance is then proportional to the auto-covariance of the primary variable:

$$C_{12}(h) = \frac{C_{12}(0)}{C_{11}(0)} C_{11}(h) \quad (4)$$

where C_{12} is the cross-covariance between the two variables Z_1 and Z_2 and C_{11} is the covariance of the primary variable Z_1. Whereas the MM2 was developed for the case where the volume support of the secondary variable is larger than that of the primary variable (Journel, 1999). This is often the case with remote sensing and seismic-related data. The more relevant Markov-type hypothesis is now:

$$E\{Z_1(u) \mid Z_2(u); Z_2(u+h) = E\{Z_1(u) \mid Z_2(u)\} \quad (5)$$

The cross-covariance is now proportional to the auto-covariance of the secondary variable:

$$C_{12}(h) = \frac{C_{12}(0)}{C_{11}(0)} C_{22}(h) \quad (6)$$

MM2 was chosen and selected because the secondary variable has larger number than that of the primary variable which is radon gas concentrations itself. Because the number of shallow drill hole points were limited in 17, the anisotropic behavior of the semivariogram was not directly determined. All the semivariogram were omni-directional without consideration of the direction that connected a point pair.

4 Result and Discussion

4.1 Lineament Densities

Lineament extraction process from the DEM data and m-STA is based on providing illumination with a direction of 0-180° and 180-360° and illumination interval of 30°. The lighting height is 50-70°. The result lineament map highlight two dominant directions, N85°E and N315°E, as shown in the rose diagram. These two lineament maps then were merged into one by grouping process to connect short lineaments and eliminated overlapping lineaments (Figure 4). The direction N 315° E correspond to the major directions of the local faults and fracture in the PGF.

By dividing the study area into grid-cells 250 × 250 m, 100 × 100 m, and 50 × 50 m in unit size, three types of lineament density were used Lineament Frequency Density [LFD (counts/km^2)], Lineament Length Density [LLD (km/km^2)], and Lineament Intersection Density [LID (counts/km^2)] as shown at Figure 5. All the density maps show similar trends with high densities concentrated in northeast and southeast and relatively high-density zones distributed with dominant

lineament directions. The lengths of 519 lineaments range from 0.147 to 1.582 km, with a median of 0.657 km, and generally follow a normal distribution.

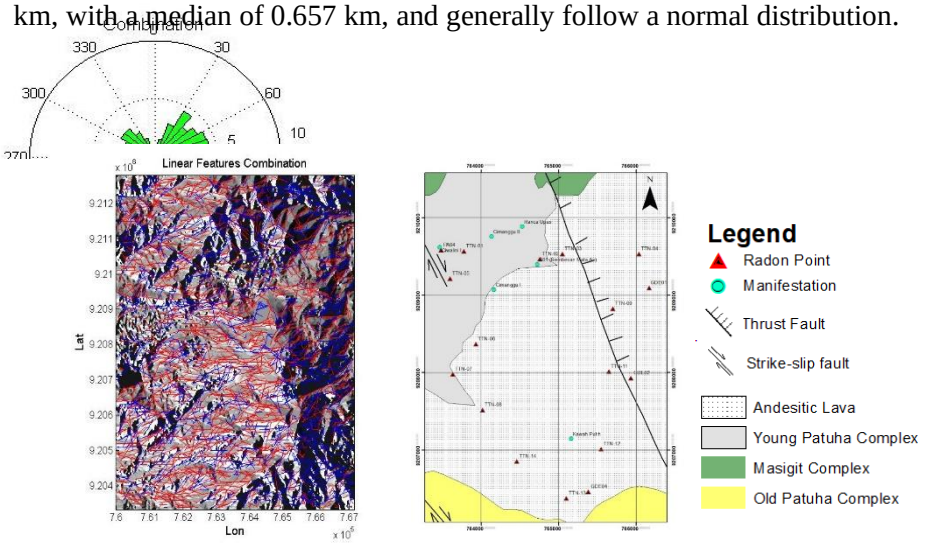

Figure 4 Lineament distribution extracted from the DEM and rose diagram of lineament directions showed in geological and local fault map of PGF.

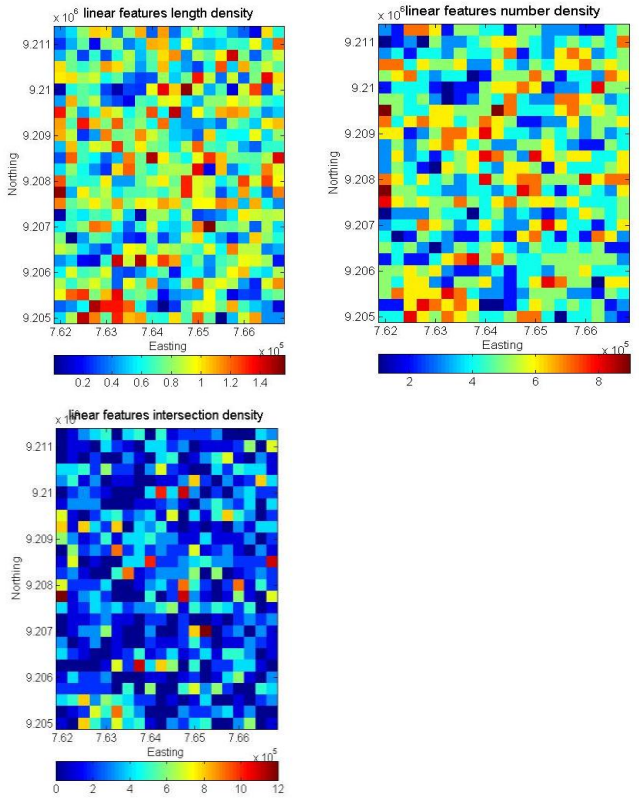

(a) (b) (c)

Figure 5 Three types of lineament density maps: (a) Lineament Length Density [LLD (km/km^2)], (b) Lineament Frequency Density [LFD (counts/km^2)], and (c) Lineament Intersection Density [LID (counts/km^2)].

4.2 Radon Gas Concentration vs. Lineament Densities

To identify correlation between radon and lineament density, statistical summary by primary and secondary were analyzed first. These statistical summaries can be shown respectively at Tables 1 and 2.

Table 1 Statistical summary of Rn concentration data used as the primary variable.

No	Radon point	Mean	Median	Q1	Q3	IQR	Maximum
1	GDE01	143.31	135	119.93	162.73	42.8	210
2	GDE02	1459.17	1544.17	1090	1886.66	796.66	1986.67
3	GDE04	1975.36	1862.02	1271.26	2424.58	1153.32	3795.71
4	PA04	4581.08	4336.47	4121.43	5343.75	1222.32	5370
5	TTN-01	3428.98	3155	2899.12	4095.83	1196.71	4970
6	TTN-02	3339.03	2946.67	2557.5	4490	1932.5	4760
7	TTN-03	5965.51	5770.36	5315.89	6676.25	1360.36	7486.67
8	TTN-04	2950.54	3233.33	2200	3865	1665	4251.67
9	TTN-05	2722.78	2697.5	1880.56	3553.39	1672.83	3808.57
10	TTN-06	1504.88	1108.75	777.13	2628.75	1851.62	3100
11	TTN-07	3612.08	3265	2668.75	4902.5	2233.75	5343.33
12	TTN-08	2734.94	2602.50	2266.11	3270	1003.89	3520
13	TTN-09	2253.61	2215	2011.67	2430.42	418.75	2756.67
14	TTN-11	2989.67	2740.83	2469	3759.17	1290.17	4075
15	TTN-12	1244.37	1178.33	931.25	1755	823.75	1761.67
16	TTN-13	1526.67	1643.33	1166.67	1781.67	615	1783.33
17	TTN-14	1819.43	1492.86	887.14	2915	2027.85	3353.33

Table 2 Statistical summary of lineament density as the secondary variable.

No	Density	Mean	Median	Q1	Q3	IQR	Maximum
1	LFD	4.53	5	3	6	3	9
2	LLD	0.74	0.73	0.51	0.95	0.44	1.56
3	LID	2.49	2	1	4	3	12

By these statistical parameters, to model permeable zones in PGF we considering by the highest correlation, the correlation coefficient (R) between Rn concentration and lineament density which is trying in three types of block size model as shown in Table 3. The highest correlation showed in 50 × 50 m on Q1 (0.45) and mean (0.4) data.

Table 3 Linear correlation coefficient between Rn concentration data and the three types of lineament density.

Block Size (m)	Correlation Coefficient	Mean	Median	Q1	Q3	IQR	Maximum
250 × 250	LFD	0.044	0.071	0.053	0.027	-0.044	0.06
	LLD	-0.007	0.017	0.014	-0.057	-0.18	0.032
	LID	-0.028	-0.077	-0.056	0.002	0.127	0.063
100 × 100	LFD	-0.13	-0.24	-0.17	-0.05	0.23	-0.021
	LLD	-0.19	-0.274	-0.24	-0.092	0.28	-0.08
	LID	0.0044	-0.146	-0.083	0.176	0.64	0.193
50 × 50	LFD	0.4	0.43	0.451	0.33	-0.12	0.36
	LLD	0.346	0.353	0.413	0.246	-0.25	0.26
	LID	0	0	0	0	0	0

4.3 Spatial Distribution of Radon Gas Concentration

4.3.1 Univariate Estimation

The Estimation following statistical methods are used to analyze the relationship between each data from a population regardless of the location of the data. This univariate statistical analysis is modeled in a histogram. Rn data histogram relatively shows normal distribution with two populations data. Variance data shows Rn concentration has a nugget model in semivariogram. Omni-directional were applied to limited number of primary variable 17 data radon points and experimental semivariograms of the Rn concentration were produced using lag separation distance of 500 m (suitable with averaged spaces of radon point) and fitted to spherical mode (Figure 6). The result by OK shows high concentrations are limited to the zone around point TTN 01, TTN 05, TTN 02 and PA 04 with 3,000 – 4,800 Bq/m^3 in the north (Figure 7).

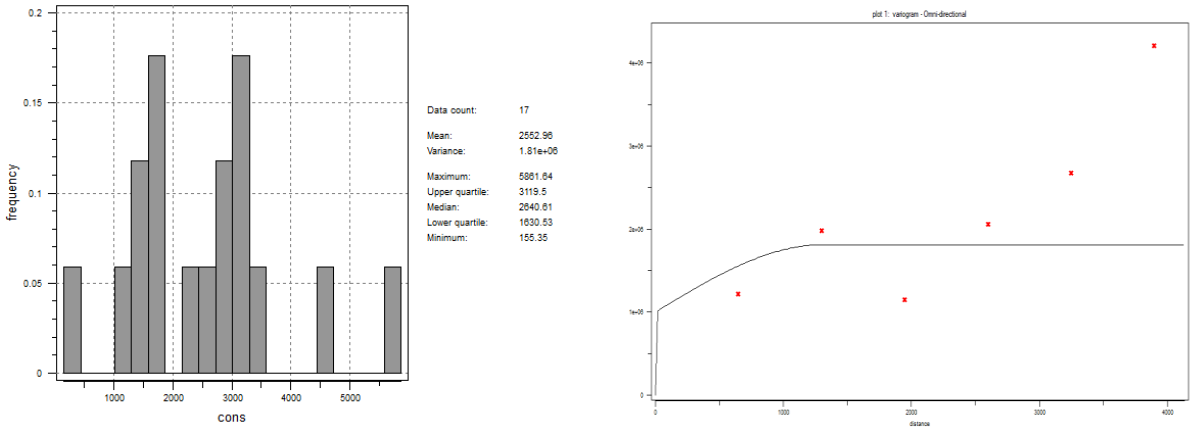

(a) (b)

Figure 6 (a) Histogram and statistical summary of Rn concentration data and (b) Variogram experimental of the averaged Rn concentration data by 17 datasets.

4.3.2 Multivariate Estimation

The result by COK shows high concentrations are limited to the zone in the north around point TTN 01, TTN 02, and TTN 03 and graded with Rn concentrations 4,165 – 5,966 Bq/m^3. Low concentrations were distributed in southern site (Figure 7).

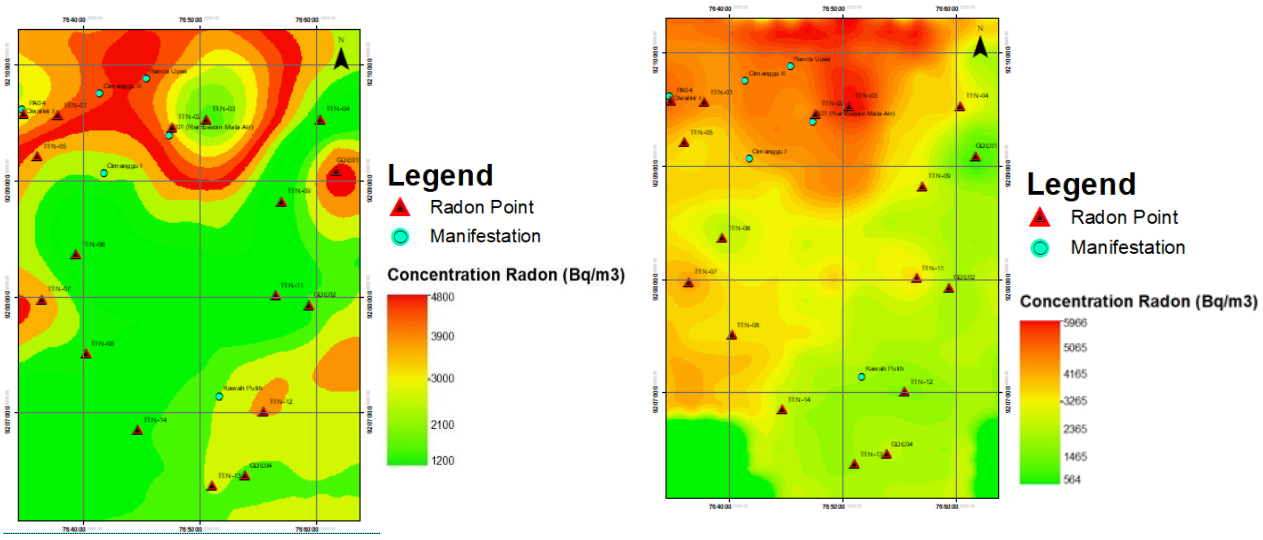

(a) (b)

Figure 7 Distribution of radon gas concentrations estimated by: (a) Ordinary Kriging (OK) and (b) Ordinary Cokriging (COK) methods at PGF.

4.4 Validation

To validate result in estimation, a cross validation was generated and showed that measurement radon (Bq/m^3) vs estimation have R value respectively 0.508 and 0.514 by modeling had been estimated using COK.

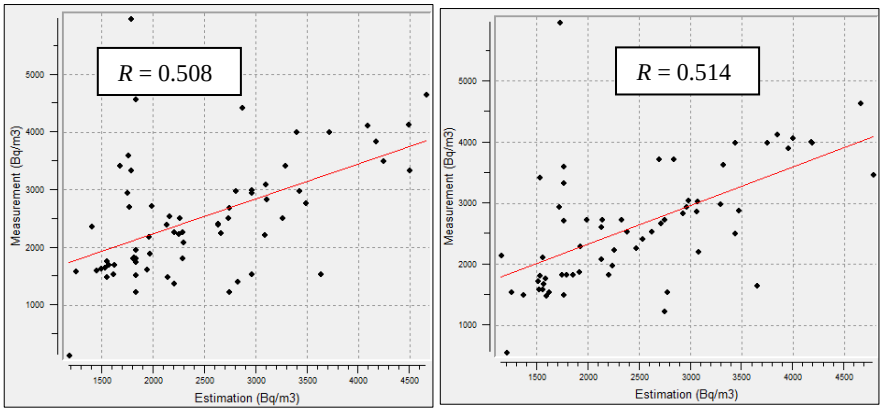

(a) **(b)**

Figure 8 Cross-plot of radon gas concentrations between the COK estimation and field measurement through secondary variable of: (a) lineament frequency density, (b) lineament length density.

5 Conclusion

This study aimed to detect permeable zones using a combination of point data of radon gas concentrations (Rn) and grid cell data of lineament density through the geostatistical method of Ordinary Kriging (OK) and Ordinary Cokriging (COK) in Patuha Geothermal Field (PGF). The main result are:

1. Lineament extraction process from the DEM data and m-STA is based on providing illumination through combination and grouping lineament map shows dominant lineament directions N85°E and N315°E and correspond to those of local faults.
2. Three types of lineament density (frequency, length, and number of intersections was modeled in grid cell 50 × 50 m because the relatively effective of moderate linear correlation coefficient (0.4) between Rn concentration data and lineament density.
3. The result by OK method shows high concentrations limited to the zone around point TTN 01, TTN 05, TTN 02 and PA 04 ranging 3,000 to 4,800 Bq/m^3 in the northern site, whereas COK method around point TTN 01, TTN 02, and TTN 03 shows higher concentrations ranging 4,165 to 5,966 Bq/m^3. In general, the low concentrations are distributed in southern site.

Acknowledgement

We are sincerely grateful for the collaboration and support from the research project of Accelerating Social Implementation for SDGs Achievement (aXis) of Beneficial Advanced Geothermal Use System (BAGUS) between Kyoto University and Bandung Institute of Technology (ITB). We also thank to PT Geo Dipa Energy (Persero) for supporting during field observation to collect the dataset. We also thank for the financial support from the Faculty of Mining and Petroleum Engineering ITB through PPMI 2021 research scheme.

References

[1] Brogi, A. & Novellino, R., *Low Angle Normal Fault (LANF)-zone architecture and permeability features in bedded carbonate from inner Northern Apennines (Rapolano Terme, Central Italy)*. Tectonophysics **638**(1), pp. 126–146, 2015. https://doi.org/10.1016/j.tecto.2014.11.005

[2] Diaz, E.G. & Arias, O.M.M., *Structural assessment and geochemistry of thermal waters at the Cerro Machin Volcano (Colombia): an approach to understanding the geothermal system*. J. Volcanol. Geotherm. Res., **400**, pp. 1–14, 2020. https://doi.org/10.1016/j.jvolgeores.2020.106910

[3] Heriawan, M.N., Syafi'i, A.A., Saepuloh, A., Kubo, T. & Koike, K., *Detection of Near Permeable Zones Based on Spatial Correlation Between Radon Gas Concentration and DTM- Derived Lineament Density*. Natural Resources Research, **30**, pp. 2989–3015, 2021.

[4] Hook, S.J, Elvidge, C.D., Rast, M. & Watanabe, H., *An evaluation of short-wave infrared (SWIR) data from the AVIRIS and GEOSCAN instrument for mineralogical mapping at Cuprite*, Nevada: Geophysics, **56**(9), p 1432-1440, 1991.

[5] Journel, A.G. & Hujibregts, C.J., *Mining Geostatistics*, New York, Academic Press., 1978.

[6] Journel, A.G., *Fundamentals of Geostatisticin Five Lesson*, **8**, Short Course in Geology, Waashington,D.C. American Geophysical union, 1989.

[7] Journel, A.G., *Markov Models for Cross Covariances*. Mathematical Geology, **31**(8), pp. 955-964, 1999.

[8] Koike, K., Nagano, S. & Ohmi, M., *Lineament analysis of satellite images using a Segment Tracing Algorithm (STA)*. Computer and Geoscience, **21**(9), pp. 1091-1104, 1995.

[9] Koike, K., Yoshinaga, T. & Asaue, H., *Characterizing long-term radon concentration changes in a geothermal area for correlation with volcanic earthquakes and reservoir temperatures: A case study from Mt. Aso, southwestern Japan*. Journal of Volcanology and Geothermal Research, **275**(1) April 2014, 85-102, 2014.

[10] Masoud, A.A. & Koik, K., *Morphotectonics inferred from the analysis of topographic lineaments auto detected from DEMs: application and validation for the Sinai Peninsula*. Egypt. Tectonophys., **510**, pp. 291-308, 2011.

[11] Moon, W. M., Chung, C.F. & An, P., *Representation and Integration of Geological, Geophysical* a*nd Remote Sensing Data*. Geoinformatics, **2**(2), pp.177-182, 1991.

[12] Morris, A., Ferrill, D.A. & Henderson, D.B., 1996. Slip-tendency analysis and fault reactivation. Geology, **24**(3), March, pp. 275–278, 1996.

[13] Nielson, D.L., 1997. Rock permeability in high-temperature geothermal systems. Proceedings of the Intersociety Energy Conversion Engineering Conference, 1837–1839, 1997.

[14] O'Leary, D.W. & Simpson, S.L., Remote Sensor application to tectonism and seismicity in the northern part of the Mississippi Embayment; Geophysic, **42**(3) pp. 542-548, 1997.

[15] Pambudi, N.A., *Geothermal power generation in Indonesia, a country within the ring of fire: Current status, future development and policy*. Journal of Renewable and Sustainable Energy, **81**(2), January, 2893-2901, 2018.

[16] Raharjo, I.B., Allis, R.G. & Chapman, D.S., *Volcano-hosted vapor-dominated geothermal systems in permeability space.* Geothermics, **62**, pp. 22-32, 2016.
[17] Rowland, J.V. & Sibson, R.H., *Structural controls on hydrothermal flow in a segmented rift system, Taupo Volcanic Zone, New Zealand*. Geofluids **4**(4), pp. 259–283, 2004.
[18] Saepuloh, A., Haeruddin, H., Heriawan, M.N., Kubo, T., Koike, K. & Malik, D., *Application of lineament density from dual orbit of synthetic aperture radar (SAR) images to detecting fluids paths in the Wayang Windu geothermal field (West Java, Indonesia)*, Geothermics, **72**, pp 145-155.
[19] Saepuloh, A., *Prinsip dan Aplikasi Penginderaan Jauh Geologi Gunung Api: Pendekatan Fisis dan Observasi Geologi Lapangan*. ITB Press., 2020.
[20] Sriwana, T., Bergen, V. & Darma, S., 2001. *Penyebaran unsur kimia dari daerah kenampakan panas bumi dan lumpur belerang di gunung Patuha, Ciwidey, Jawa Barat.* In: The 5th Inaga Annual Scientific Conference and Exhibitions. INAGA, Indonesia, Yogyakarta, 2001.
[21] Suswati, Mulyana, A.R., Haerani, N. & Sutawidjaja, I.S., *Pemetaan geologi komplek gunungapi Patuha, Kabupaten Bandung, Jawa Barat. Direktorat Vulkanologi,* Unpublished, Bandung, KESDM, 2001.
[22] [Tamanyu, S., Fujiwara, S., Ishikawa, J.I. & Jingu, H., *Fracture system related to geothermal reservoir based on core samples of slim holes*. Example from the Uenotai Geothermal Field, northern Honshu, Japan. Geothermics, **27**(2), pp. 143–166, 1998.
[23] WestJEC, 2007. *Feasibility study for Patuha geothermal power development.* Japan Bank International Cooperation (Unpublished).
[24] Whitehead, N.E., 1981. A test of radon ground measurements as ageothermal prospecting tool in New Zealand. N.Z. J, Sci 24(1): pp 59-64.
[25] Whitehead, N.E, 1984. Geothermal Prospecting by Ground Radon Measurement. Journal of Vulcanology and Geothermal Research, 20, 213-229, 1984.
[26] Wackernagel, H., 2003. Multivariate Statistics, Berlin, Springer-Verlag.